A Compact Two-Port Handset MIMO Antenna with High Isolation for 5G mm-Wave Applications

Watheq A. Neamah [1, 2] *, Haider M. Al Sabbagh [1], and Hussain Al-Rizzo [3]

[1] Department of Electrical Engineering, College of Engineering, University of Basrah, Basrah, Iraq
[2] College of Engineering, University of Thi-Qar, Iraq
[3] Department of Systems Engineering, University of Arkansas University Little Rock, Little Rock, AR, USA
* Correspondence: watheq.neamah@utq.edu.iq (W.A.N.)

***Abstract*— In this paper, a novel design of a compact coplanar waveguide (CPW) fed multiple-input-multiple-output (MIMO) handset antenna operating in a wide frequency range at the 5G New Radio (NR) millimeter wave (mmWave) band extending from 23.5 GHz to 41 GHz. The planar geometry results in a small, compact structure with a wide operating bandwidth, high gain, and high radiation efficiency. The utilized antenna was a single-layer surface-mounted CPW in a pin-clamp-like (PCL) structure fed with a wide ground slot. The two-element MIMO antenna consists of closely-spaced parallel elements placed $\lambda_0/16$ apart from the closest edge, wherein λ_0 is the free space wavelength at the 28 GHz operating frequency. A novel inverse S-shaped (IS) decoupling strip structure was used. The proposed antenna element was designed on a Rogers RT5870 substrate using CST Microwave Studio and further validated using Ansys HFSS software. The simulated frequency bandwidth was confined to (23.5-41) GHz, showing both software good agreement results. At 37 GHz, the antenna array provides a maximum simulated gain of 6.6 dBi, while its lowest was 1.5 dBi at 24 GHz, and its minimum radiation efficiency was 93% over the whole band. This array revealed excellent MIMO performance metrics, such as envelope correlation coefficient ECC, diversity gain DG, and mean effective gain MEG, of excellent results, making this array a good choice for emerging 5G communications applications.**

***Keywords*—Two ports, MIMO, 5G, mmWave, high isolation, ECC**

I. Introduction

The rapid progress of cellular wireless communication systems has increased the importance of similar developments in the design of modern antenna systems, which are essential components of any wireless device. The ever-increasing has greatly influenced the current telecommunication system, increasing data consumption and demand for faster data speeds. To address the increasing demand for faster and more reliable connectivity, researchers are exploring new 5G communication technologies. The World Radio-communication Conference (WRC) has allocated many mmWave frequencies for future 5G systems since they provide a high data rate [1].

5G is focused on the centimeter and mmWave spectrums, which may enable attaining the larger bandwidth with a data rate of several Gbps. There are several advantages of using these frequencies: The lower portion of the spectrum has already been occupied by many different types of wireless networks and applications, such as Wi-Fi, WiMAX, Bluetooth, and industrial, scientific, and medical (ISM), while the upper portion is mainly underutilized and ready for 5G technology [2]. The 5G spectrum is addressed by many countries, as shown in Fig. 1. 5G networks using multiple-input-multiple-output (MIMO) as an enabling technology to provide significant improvements in channel capacity, data rates, latency, efficiency, link reliability, and energy conservation compared to single input, single output (SISO) systems [3], [4], without increasing the power or bandwidth. Wireless communication systems are influenced by multipath fading. MIMO technology is one solution for taking advantage of multipath fading by operating multiple independent data sub-channels. Thus, wide bandwidth MIMO technologies are critical to 5G systems and beyond because they can use the multipath feature to maximize spectrum efficiency and channel capacity without increasing power transmitted [5, 6]. For a desirable performance, a MIMO system should also have strong isolation among the transmitting and receiving antenna elements and wideband properties [7]. An increase in the inter-element mutual coupling might degrade the performance of a MIMO antenna system. Developing a miniaturized MIMO antenna system with a high element isolation level while having a common ground structure is a challenging design problem [8].

The researchers devised many ways to increase the isolation among antenna elements in MIMO applications. These include stubs, Defected Ground Structure (DGS), Electronic Band Gap (EBG), and Split Ring Resonator (SRR), among other techniques [9–12]. A dipole with V-shaped branch ground [13] or a monopole antenna with SRR and ground with a ring-shaped resonator was utilized

Manuscript received July 21, 2023; revised August 22, 2023, accepted September 10, 2023.

for wide-bandwidth MIMO antennas [14]. It should be noted, however, that it is desired that MIMO antennas must have common ground among the components for practical applicability. Single and dual frequency band two-port mmWave MIMO antennas are presented; in [15], the design has a common ground profile, and in [16], a separated ground structure is utilized.

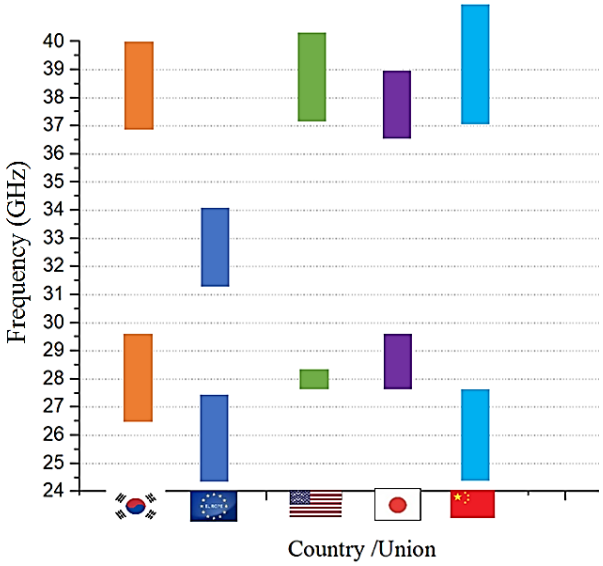

Figure 1. International allocations of 5G spectrum [3].

In [17], a modified W-shaped antenna provides sub-6 and mmWave operation. In [18], a hybrid model is proposed, consisting of a 2×1 array for sub 6 based on a single-element antenna for mmWave application. In [19], the authors proposed an antenna comprising two collinear printed dipoles to cover 17.5 GHz of 24.6 GHz to 46.1 GHz and 2.4 GHz of 50.1 GHz to 52.5 GHz bandwidths of mmWave bands. Moreover, mmWave substrate that mode suppression is critical to achieving acceptable efficiency. The first strategy is to keep the thickness of the substrate (h) 0.01 times the operating wavelength at the lowest operating frequency to attain an efficiency greater than 90 % [20]. Furthermore, the surface modes can be grounded using metallic vias utilizing substrate-integrated waveguide (SIW) or λ_0 gap between array components [21]. However, this technique has a narrow bandwidth and increases the fabrication complexity and overall weight because of the additional metallic contacts.

This paper presents a compact, high-isolation, two-port MIMO antenna that aims to cover a wide frequency range in the mmWave band, extending from 23.5 GHz to 41 GHz and meets the new 5G technology of MIMO radiators with high radiation efficiency. The single element consisted of a pin clamp-like (PCL) conductor based on a CPW strip feed. The ground had a wide rectangular (5.2×4) mm^2 slot cut in its top left corner. Over the operating frequency range, more than 90% radiation efficiency was achieved. The proposed MIMO antenna had a small footprint (10.8×8×0.8) mm^3 and comprised two ports with more than 22 dB isolation over the whole frequency band. The isolation structure between the antenna elements comprised a simple inverse S (IS) shape, which also acted as a common ground. All MIMO performance metrics like ECC, Diversity Gain (DG), radiation efficiency, antenna gain, and Mean Effective Gain (MEG) were discussed in detail. The excellent MIMO performance metrics demonstrated for the proposed antenna make it a good candidate for the 5G mmWave application.

The rest of the paper is organized as follows. Section II particulars the single antenna design procedure. Section III deals with MIMO elements and isolation. Section IV compares the design performance against existing designs. Section V is the conclusion.

II. The Single Antenna Element

A. Design Procedure

Fig. 2(a) shows that a single antenna element consisted of a rectangle ground slot of (5.2×4) mm^2 that surrounds a radiator with a square slit on its top. As shown in Fig 2(b), a cut was made at the radiator on the right side of the square slot to increase the disturbance of the routing path of the surface current. A DGS was applied in the upper left corner of the ground to expand the frequency response band; this can be seen in Fig. 2(c). The design process and parametric study are to be explained in the following subsections.

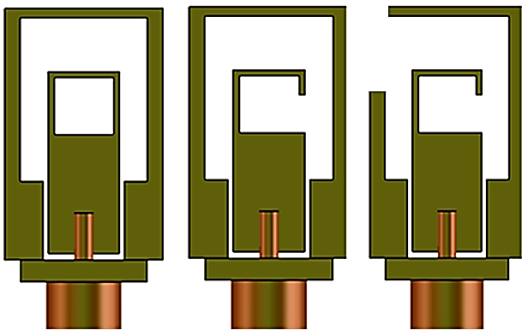

(a) (b) (c)

Figure 2. mmWave single element design procedure; (a) Antenna 1 (b) Antenna 2 (c) Antenna 3.

Fig. 3 illustrates the single footprint of the investigated PCL antenna. A 50-ohm SMA connector feeds the antenna. The antenna element comprises a strip line terminated by a wide square slot patch and a wide ground slot surrounding the patch. The patch and ground planes are constructed on the same side of a Rogers RT5870 substrate with a dielectric constant (ε_r) of 2.33, a thickness (h) of 0.8 mm, and a loss factor of 0.0012, while the other side is copper-free. The monopole antenna, depicted in Fig. 3, is fed with a CPW strip line of width W_1. The formula used in the initial design of the single element is listed below [22]:

$$L = \frac{c}{2f_r\sqrt{\varepsilon_{eff}}} \quad (1)$$

Wherein L is the length of the radiator, f_r is the resonance frequency, c is the speed of light, and ε_{eff} is the effective dielectric constant.

$$\varepsilon_{eff} = \frac{\varepsilon_r + 1}{2} \quad (2)$$

ε_{eff} is the relative dielectric constant.

Table I depicts the overall dimensions of the final design.

TABLE I. ANTENNA PARAMETERS

Parameters	Value(mm)	Parameters	Value(mm)
W	5	*L*	8
W1	2.25	*L1*	5.70
W2	0.73	*L2*	5.20
L3	3.2	*L4*	3.5
L5	1.8	*L6*	0.7
T1	0.2	*T2*	0.15
T3	0.3	*LC*	2

B. Radiator Cut Parameter Effect

The first parameter of the antenna construction was a wide cut made in the radiator section. This study examined the disturbance in the surface current to make the antenna as compact as possible while contributing to extending the frequency bandwidth. A parametric sweep simulation used CST Microwave Studio to enhance the frequency bandwidth in the desired mmWave range. The parameter L_6 represents the slot etched on the radiator side.

Fig. 4 shows the parametric sweep of the etched slot parameter values, starting at L_6 = 0.8 mm and ending at L_6 = *2* mm. The scattering parameter S_{11} expressed the reflection coefficient, which the slot parameter examines versus frequency. As shown in Fig. 4, the optimal result was achieved when L_6 equals 0.8 mm, wherein the bandwidth for S11<-10 dB for the frequency band from 28.5 GHz to 38 GHz.

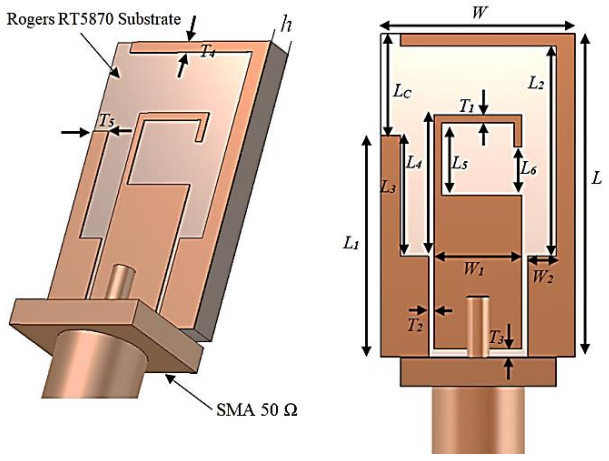

Figure 3. Single antenna configuration.

C. Effect of Ground Cut Parameter

The last frequency response did not satisfy the intended band, so further investigation is needed to enhance antenna response. Hence, the second parameter of the structure is another investigated by an etched slot in the ground ring denoted by (*Lc*) at the top corner for further enhancement in bandwidth range. The parameter L_C is swept from 0.5 mm to 2.5 mm. Fig. 5 shows the optimum response value at 2 mm, wherein the frequency response over which S_{11}<-10 dB extends from 22 GHz to 41 GHz. This response covered all frequency bands allocated for the new radio NR of mmWave in 5G.

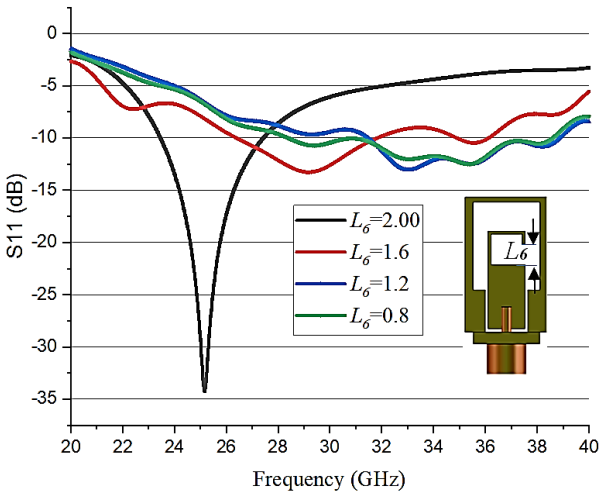

Figure 4. L_6 parameter effect investigated.

D. Validation of the Simulated Impedance Bandwidth of the Single Element with HFSS Software

A High-Frequency Structure Simulator (HFSS) was utilized to validate the design results. The HFSS relies on the finite element method, whereas the CST simulator relies on the finite integration technique. The perfect match layer (PML) boundary condition for the CST simulation had a fractional wavelength minimum distance from the structure of 4 and a center frequency of 29 GHz.

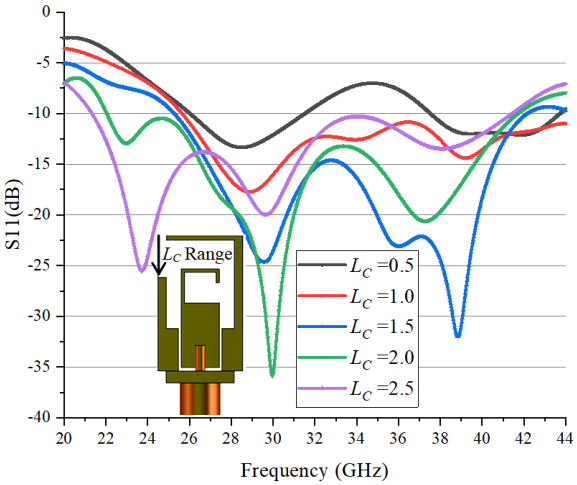

Figure 5. L_C parameter effect investigated.

PLM was proved to be an excellent absorbing boundary condition (ABC). The mesh characteristics of the simulation were conducted with a hexahedral solver. HFSS, on the other hand, used the integral equation (IE) domain as the radiation boundary. The HFSS-IE domain used integral equation formulation, a precise condition for transparency. Using conformal radiation volumes of the IE boundary, which decreased the total finite element solution

domain, a more accurate simulation of an electrically large open boundary was attained.

As shown in Fig. 6, the S_{11} bandwidth for which less than -10 dB from CST was between 22 GHz to 41 GHz, while from HFSS was between 23.5 GHz and 41.5 GHz, exhibiting notable agreement of bandwidth that was consistent with the majority of new 5G spectrum responses. Although both software used different calculation techniques, their S-parameter results were almost identical.

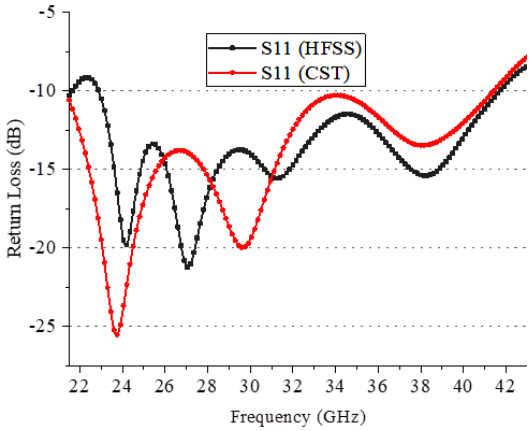

Figure 6. CST and HFSS return loss validation.

III. Design of the Proposed MIMO Antenna Array

In this section, this study investigates the side-by-side orientation of the two-element MIMO antenna and the approach utilized to minimize mutual coupling. As shown in Fig. 7, the configuration is intended to illustrate the effect of element orientation on matching and isolation between the antenna ports. The minimum separation between the closest metal body of the MIMO antennas was fixed as S= λ_0/16 mm, wherein the wavelength is calculated at 28 GHz in free space.

Three scenarios of the side-by-side layouts were investigated. Fig. 7 (a) shows a scenario of the mirror face layout. The S-parameters are shown in Fig. 8(a) for this layout. Although the responses of S_{11} and S_{22} are acceptable, the isolation does not satisfy the acceptable MIMO criterion.

Fig. 7(b) shows the mirror face layout, its response, and the isolation between antennas shown in Fig. 8(b). With this layout, the S_{11} and S_{22} are acceptable over the whole frequency response, but the isolation between 26.5 GHz to 34 GHz was less than 20 dB; again, the isolation did not satisfy the acceptable MIMO criterion.

Fig. 7(c) shows the successive layout, its response, and the isolation between antennas shown in Fig. 8(b). The isolation between antennas with this layout was improved over the whole frequency response except for the band between 24.5 GHz to 26.4 GHz is less than 20 dB. Besides, in the $S_{22,}$ a notch was observed at the band between 29.4 GHz to 31 GHz due unsymmetrical layout. Although the isolation was enhanced, the response was notched in S_{22} along the band response. Also, the isolation did not cover greater than or equal to 20 dB over the targeted band. In addition, the side-by-side layout, as discussed, does not include the common ground of the antenna element. Hence, the coming subsection will discuss the decoupling and common ground structure.

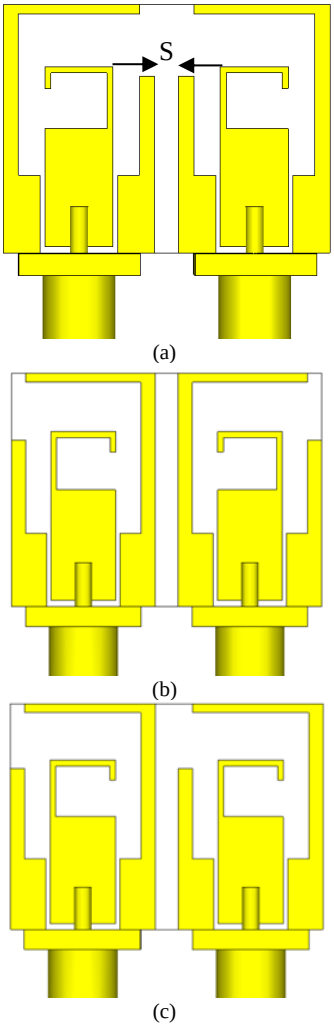

Figure 7. Side-by-side MIMO antenna scenarios: (a) mirror face layout, (b) opposite face layout, and (c) successive layout.

A. Decupling Structure Analysis

A simple decoupling approach was introduced to achieve isolation better than 20 dB and to restore the frequency response for the two ports so that the results approach of the single element response. Moreover, a common ground was also needed to make the proposed MIMO antenna more practical.

As shown in Fig. 9, an inverted S-shaped (IS-shape) was proposed as the decoupling structure. The IS-shaped structure was deployed between the closely spaced radiating elements to induce a surface current that opposes that induced due to mutual coupling and hence eliminates electromagnetic coupling as observed at port 2 when port 1 is excited. This field cancellation affected the antenna input impedance and reduced coupling across antenna ports. The parametric analysis was conducted to achieve optimal isolation by varying the parameter *H* representing the IS-shape height. The parameter *SW* was the step width, fixed at 0.3 mm.

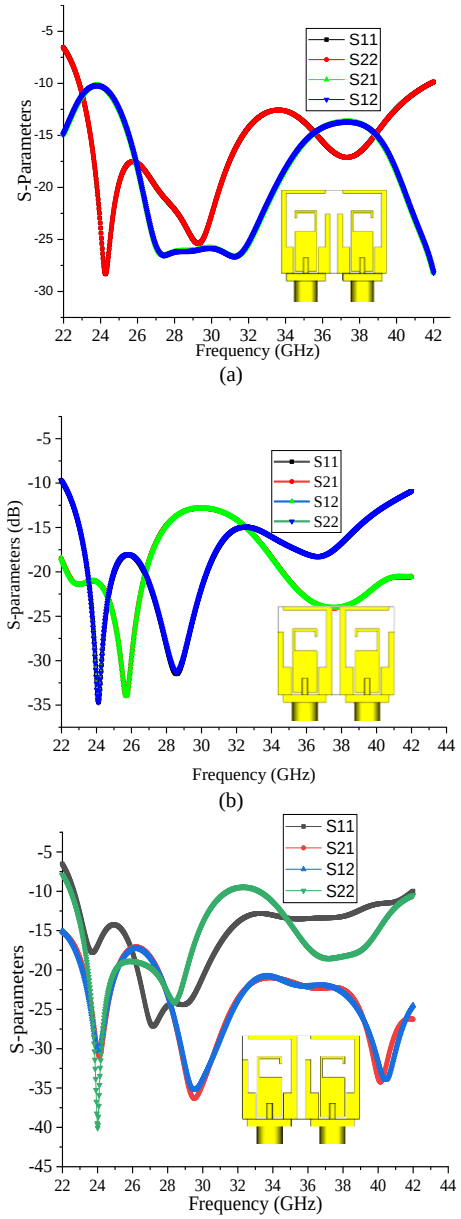

Figure 8. Side-by-side MIMO antenna S-parameters: (a) mirror face layout, (b) opposite face layout, and (c) successive layout.

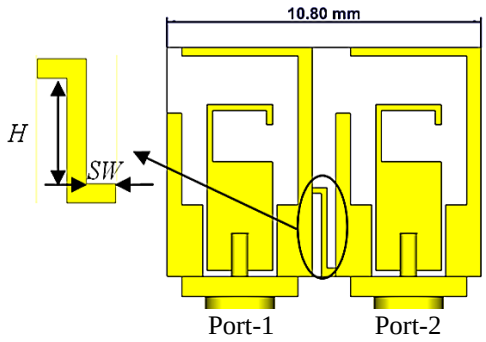

Figure 9. Inverse S-shaped decoupling structure.

As shown in Fig. 10 (a), the parameter of the height of strip (*H*) affected both the matching and isolation. Three values of *H* are swept starting from 0 mm, representing a straight line connecting both antennas, and other values are 0.9 mm and 3 mm, respectively. The sweep is shown for three different values of *H* to prevent the figure from becoming overcrowded with curves. At *H*=0.9 mm, the response of S_{22} is enhanced. However, the S_{11} is slightly notched. As shown in Fig. 10(b), the isolation was confined to 24.8 -28 GHz with an isolation of less than 20 dB. At *H*=1.8 mm, the isolation was enhanced, and S_{11} was slightly enhanced. At *H*=2.7 mm, the response for both ports was confined to bandwidth from 23.5 GHz to 41 GHz for S_{11}<-10 dB. The isolation was better than 22 dB for the whole bandwidth.

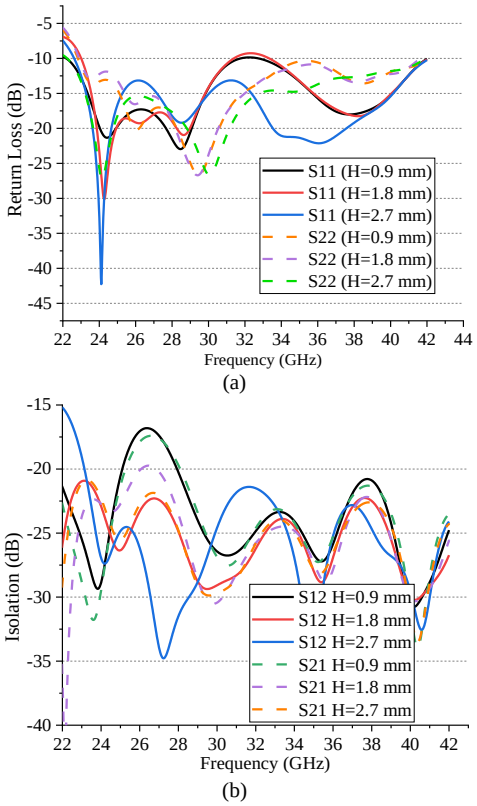

Figure 10. IS-shaped *H* parameter of decoupling: (a) Return Loss and (b) Isolation.

HFSS software was used to verify the simulation findings with CST. In the next part, further elaboration on this validation is presented.

B. Numerical Results and Analysis

HFSS validated the frequency response of the matching and isolation. Fig. 11 shows the return losses of two-element MIMO antenna results in both software. As shown in Fig. 11(a), the return losses were in close agreement using both software tools wherein the bandwidth is confined to (23.5 – 41) GHz. Both ports' isolation depicted in Fig. 11(b) was better than 22 dB using both software.

As shown in Fig. 12, the antenna realized gain was simulated using CST and validated using HFSS. The realized gain was 1.5 dBi at 24 GHz, increasing to 6.5 dBi at 38 GHz for the two-element MIMO antenna using CST software, which was in close agreement with HFSS. Fig. 12 on the right side also displays the simulated radiation efficiency of the proposed two-element MIMO antenna.

According to the research results of [23], if the design structure of the antenna could ensure the current flowing through it remained at a comparable level, it would attain maximum efficiency. So, we devised a unique design that uses a coplanar layer with a wide uncleared area of the conductor surface (radiator and ground of copper), which gives an even current flow throughout the antenna body and maximizes the antenna efficiency.

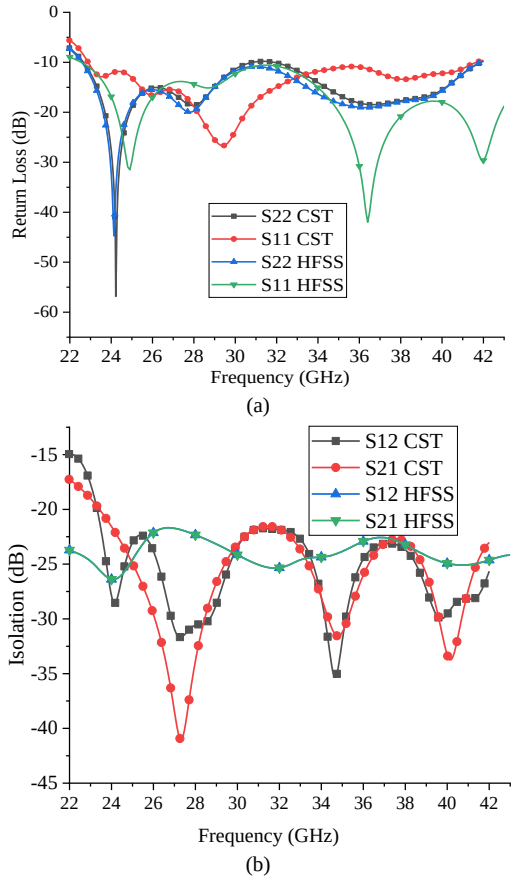

Figure 11. S-parameters validation: (a) Return Loss and (b) Isolation.

It was shown that the radiation efficiency of MIMO antennas decreased marginally. The suggested MIMO antenna had a radiation efficiency for both ports ranging from 92% to 97% throughout the frequency range (23.5-41) GHz.

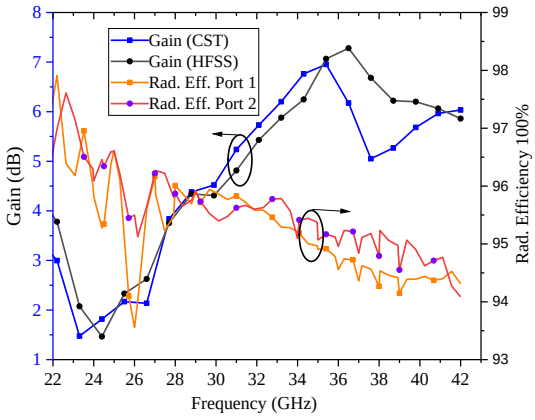

Figure 12. Simulated antenna gain and radiation efficiency.

As shown in Fig. 13, the surface current distribution is analyzed at three operating frequencies (24.5, 28.5, and 38.5) GHz to illustrate the effectiveness of the radiator and the decoupling structure. The left side of Fig. 13 represents port-1 excited, while the right side represents port-2 excited. As shown in Fig. 13(a), the current distribution shows that at a low frequency of 24.5 GHz, most radiation is intensive around the whole radiator structure in both ports due to its expressing the fundamental frequency response. Also, the IS-shaped decoupling structure and ground possess intense surface currents, suppressing the other port interaction. As the operating frequency rises, as in Fig. 13(b), the active zone of the current shifts to the base of the clamped shape radiator of the MIMO antenna. As shown in Fig. 13(c), there is also a significant current concentration at 38.5 GHz near the base of the radiator and along the edge corner. Nonetheless, it can be seen that the current concentration on the IS-shaped decoupling structure remains constant over the whole band of (23.5 – 41) GHz range between adjacent structures, which significantly reduces the mutual coupling between radiating MIMO elements. At 38,5 GHz, the IS decoupling is much more concentrated when port-2 is excited than when port-1 is excited, which plays a role in reducing coupling because of the asymmetry of the layout.

Fig. 14 depicts the simulated polar radiation patterns for port-1 and port-2 at frequencies of 24.5 GHz, 28.5 GHz, and 39.5 GHz. The developed MIMO antenna exhibits dipole-like radiation patterns at these frequencies in both the y-z plane of $\phi = 0^0$ versus θ and the x-z plane of $\phi = 90^0$ versus θ. As seen in Fig. 14 (a), (b), and (c), the MIMO antenna also provides a complementary radiation pattern in the y-z plane at ports 1 and 2 of 24.5 GHz, 28.5 GHz, and 39.5 GHz, respectively.

C. MIMO Antenna Performances

In this section, this study will provide the metrics that are vital to assessing the performance of the proposed wideband MIMO antenna. The Envelope Correlation Coefficient (ECC), the Diversity Gain (DG), and the Mean Effective Gain (MEG).

The ECC is an important indicator of the correlation between the antenna ports. As the correlation drops, the MIMO antenna may be able to handle more data with minimal interference. ECC value may be calculated by analyzing the far-field radiation pattern or the S-parameters [24].

The ECC coefficient has to be smaller than 0.5 for MIMO to work properly [25]. Using the S-parameters, if the radiation efficiency is high, the ECC is almost identical to that calculated from the radiation patterns. The authors of [26] provide the formula for calculating the ECC for a two-element MIMO antenna from the S-parameters:

$$ECC = \rho_e = \frac{\left|S_{11}^* S_{12} + S_{21}^* S_{22}\right|^2}{\left(1-\left(\left|S_{11}\right|^2 - \left|S_{21}\right|^2\right)\right)\left(1-\left(\left|S_{22}\right|^2 - \left|S_{12}\right|^2\right)\right)} \quad (3)$$

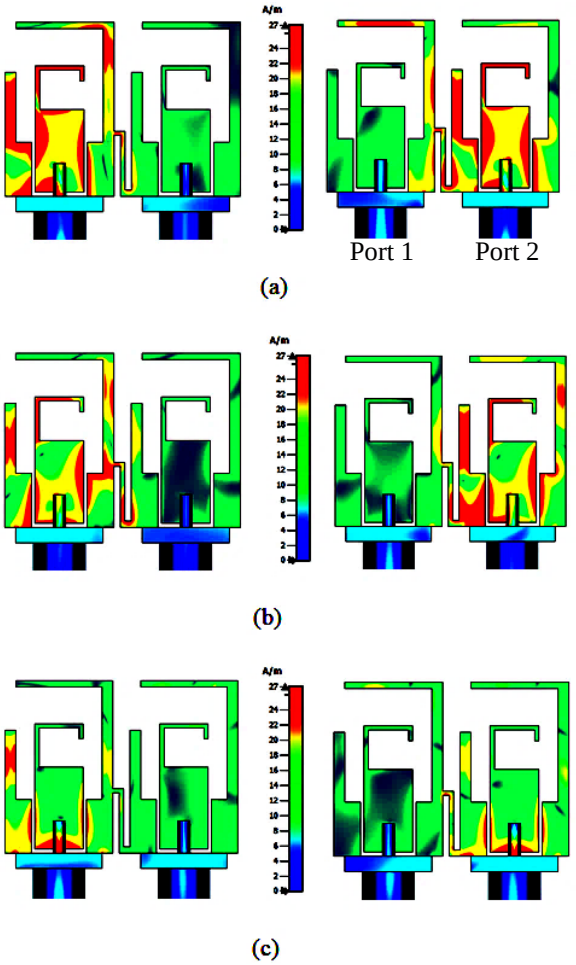

Figure 13. Surface current: (a) 24.5 GHz, (b) 28.5 GHz, and (c) 38.5 GHz.

The notations S_{11}* and S_{21}* represent the complex conjugates of S_{11} and S_{21}, respectively.

The ECC is also computed by utilizing the far field patterns, which are given by [27]:

$$ECC(\rho_e) = \frac{|\iint 4\pi[R_1(\theta,\Phi).R_2(\theta,\Phi)d\Omega]|^2}{\iint 4\pi|R_1(\theta,\Phi)|^2 d\Omega \iint 4\pi|R_2(\theta,\Phi)|^2 d\Omega} \quad (4)$$

$R_i(\theta,\emptyset)$ represents the 3D radiation pattern when antenna (i) is active, whereas $R_j(\theta,\emptyset)$ characterizes the 3D radiation pattern when antenna j is active. Ω pertains to the solid angle.

The diversity gains (DG) for two antennas with ECC = 0 is 10 dB, which refers to an increase in the reliability of the radio link. The correlation among the individual antenna elements degrades the diversity performance of a MIMO system. The approximate relationship between DG and ECC can be expressed by the equation below [28]:

$$DG = 10\sqrt{1-ECC^2} \quad (5)$$

Fig. 15 depicts the ECC calculated from the S-parameters and far-field of the proposed wideband MIMO antenna. The ECC value is less than 0.001 according to the far-field and S-parameter simulation results, with both values being almost close to one another, indicating the high efficiency of the MIMO antennas. The simulated DG value is more than 9.999 across the entire operating bandwidth. Therefore, the proposed wideband MIMO antenna has an excellent diversity performance.

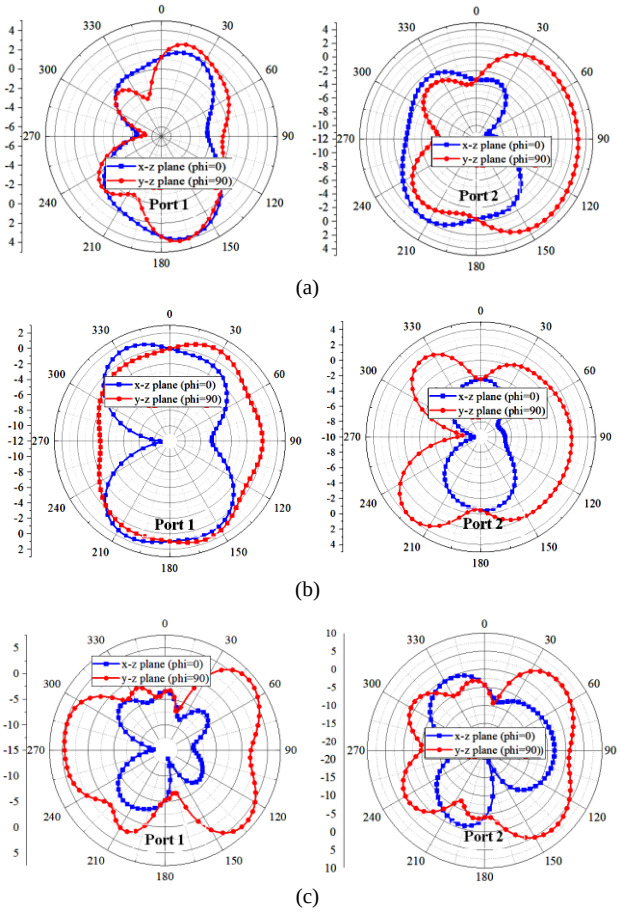

Figure 14. The radiation pattern of ports 1 and 2: (a) 24.5 GHz, (b) 28.5 GHz, and (c) 38.5 GHz.

MEG is another crucial metric in MIMO analysis, calculated as the proportion of power received in a diversity antenna to power received by an isotropic antenna. It reveals the gain performance of MIMO antennas when environmental conditions are considered. At ports 1 and 2, the MEG analysis is done on the proposed antenna. An optimal MIMO antenna design requires MEG1-MEG2 to be near zero at the same power level. MEG can be calculated from S-parameters as given below [29].

$$MEG_n = \frac{1}{2}[1-|S_{nn}|^2-|S_{nm}|^2] \quad (6)$$

$$MEG_m = \frac{1}{2}[1-|S_{nm}|^2-|S_{mm}|^2] \quad (7)$$

The S_{nn}, S_{mm}, and S_{nm} are the S parameters of (n), which refers to port 1, and (m) refers to port 2.

The optimal MEG value range is $-12 \le MEG(dB) \le -3$ [30]. As seen in Fig. 16, the MEG ports are near −3 dB, wherein the difference of MEG1-MEG-2 is almost zero. These results emphasize excellent MIMO performance.

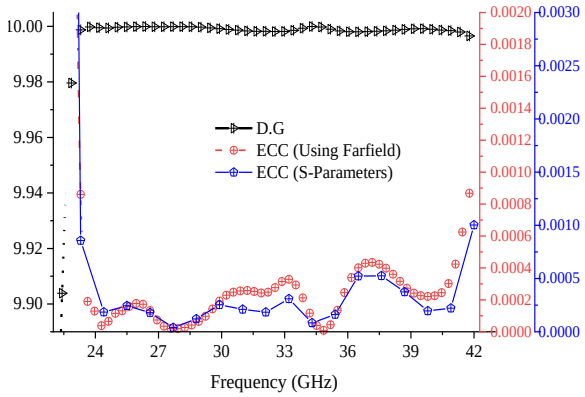

Figure 15. Antenna MIMO performance ECC and DG.

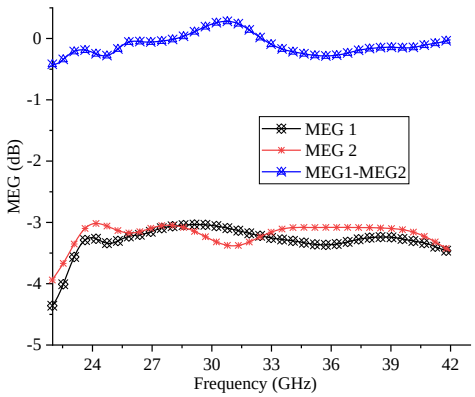

Figure 16. Mean Effective Gain of the proposed antenna.

TABLE II. COMPARISON OF SIMULATED ANTENNA WITH STATE-OF-THE-ART

Ref. No.	**Structure/ Size(mm^3)**	**Operating Frequency (GHz)/Number of Ports**	**Substrate type**	**Isolation(dB)**	**ECC/DG (dB)**	**Rad. Efficiency (%)**
Usma *et al.* [15]	Air Full Slot/33×27.5×0.76	28/**2**	TLY-5 substrate ε_r= 2.2, tanδ = 0.0009	<30	0.001/9.9998	-
Hasan *et al.* [31]	Rectangular with hemispherical contour/ 14 × 12 × 0.38	(26.65–29.2) (36.95–39.05)/**2**	Rogers RT/Duroid 5880 ε_r = 2.2, tanδ = 0.0009	<20	0.001/9.92	78/76
Sabek *et al.* [32]	Monopole with triangle and rectangular stubs/ 27.65×12× 0.273 mm^3	(26-30)(36-41.5)/**2**	Rogers RO4003 ε_r = 3.55	<30, <20	0.0001/9.99	-
Hadri *et al.* [33]	5-shaped radiating patch 12.8×26×1.6	(32.3 to 54.6)/**2**	FR4 ε_r =4.4 tanδ = 0.02	<20	0.003 /9.993	82.46
Fakharian *et al.* [34]	Planar log-periodic array 55×45×1.57	(12.82–12.98), (13.54– 13.96), (14.81–15.15), (17.7–18.52), (21.1–22.1)/**2**	RT Duroid 5880 ε_r = 2.2 tanδ = 0.0009	<23.5	0.03/9.995	72–97
Esmail *et al.* [35]	Pentagon monopole antenna 26 × 14.5 × 0.508	(26–28), (37–39)/**2**	RT Duroid 5880 ε_r = 2.2, tanδ = 0.0009	<39, <38	0.0001/9.999	92-92.2
Ahmad *et al.* [36]	Simple rectangular patch 11.4 × 5.3×0.8	(28.75–29.85)/**2**	Roger 4350B ε_r = 3.7, tanδ = 0.0037	<36	0.0001/0.98	85
This Work	Pin clamp-like 10.8×8×0.8	23.5-42/**2**	Rogers RT5870 ε_r = 2.33 tanδ = 0.0012	<22.5	0.001/9.999	92–96

IV. Performance Comparison Against Existing Designs

Table II compares this study's proposed design against typical two-port MIMO antennas reported in the literature. One can see from the table that the overall dimensions of this study's design are much smaller. Although the reported designs achieved high isolation and low ECC, they exhibit low radiation efficiency, low bandwidth, and bulky or complex design. Table II shows that the proposed MIMO antenna is compact, simple to fabricate, wide bandwidth, high radiation efficiency, excellent DG, and a low ECC.

V. Conclusion

A two-port broadband MIMO antenna array was presented for 5G communications. The proposed antenna was designed to function at wide frequency bands ranging from 23.5 GHz to 41 GHz, with isolation values larger than 20 dB throughout the entire band. The single element was a pin clamp shaped with a wide slot ground cut at the top corner excited by CPW feed. The MIMO array was aligned parallel with the Inverse S-shaped decoupling structure. The design was conducted using CST and verified against HFSS software. The overall array dimensions were $10.8\times8\times0.8$ mm^3. The results obtained from CST compared with HFSS software seem in close agreement, which validates the proposed antenna array design. The MIMO metrics, such as ECC, DG, and MEG, were evaluated and provided excellent performance.

Conflict of Interest

The authors declare no conflict of interest.

Author Contributions

Watheq A. Neamah conducted the research, designed and analyzed the data, and wrote the paper, and Haider A. Alsabage and Hussian A. Alrizo revised, modified, and edited the final copy. All of the authors have approved the final copy.

References

[1] P. R. Girjashankar and T. Upadhyaya, "Substrate integrated waveguide fed dual-band quad-elements rectangular dielectric resonator MIMO antenna for millimeter wave 5G wireless communication systems," *AEU - Int. J. Electron. Commun.*, vol. 137, p. 153821, 2021.

[2] J. Khan *et al.*, "Design and performance comparison of rotated Y-shaped antenna using Different metamaterial surfaces for 5G mobile devices," *Comput. Mater. Contin.*, vol. 60, no. 2, pp. 409–420, 2019.

[3] H. M. Marzouk, M. I. Ahmed, and A. A. Shaalan, "A novel dual-band 28/38 GHz slotted microstrip MIMO antenna for 5G mobile applications," in *Proc. 2019 IEEE Int. Symp. Antennas Propag. Usn. Radio Sci. Meet. APSURSI 2019 - Proc.*, no. c, pp. 607–608, 2019.

[4] M. Kamran Shereen, M. I. Khattak, and J. Nebhen, "A review of achieving frequency reconfiguration through switching in microstrip patch antennas for future 5G applications," *Alexandria Eng. J.*, vol. 61, no. 1, pp. 29–40, 2022.

[5] L. Sun, Y. Li, Z. Zhang, and Z. Feng, "Wideband 5G MIMO antenna with integrated orthogonal-mode dual-antenna pairs for metal-rimmed smartphones," *IEEE Trans. Antennas Propag.*, vol. 68, no. 4, pp. 2494–2503, 2020.

[6] M. Abdullah, S. H. Kiani, and A. Iqbal, "Eight element multiple-input multiple-output (MIMO) antenna for 5g mobile applications," *IEEE Access*, vol. 7, pp. 134488–134495, 2019.

[7] U. Rafique *et al.*, "Applied sciences uni-planar MIMO antenna for sub-6 GHz 5G mobile phone applications," *Applied Sciences*, 2022.

[8] D. A. Sehrai *et al.*, "A novel high gain wideband mimo antenna for 5g millimeter-wave applications," *Electron.*, vol. 9, no. 6, pp. 1–13, 2020.

[9] K. V. Babu, S. Das, S. Lakrit, S. K. Patel, B. T. P. Madhav, and H. Medkour, "Compact dual-band printed MIMO antenna with very low mutual coupling for WLAN, Wi-MAX, Sub-6 GHz 5G and X-band satellite communication applications," *Prog. Electromagn. Res. C*, vol. 117, pp. 99–114, 2021.

[10] N. Ashraf, O. Haraz, M. A. Ashraf, and S. Alshebeili, "28/38-GHz dual-band millimeter wave SIW array antenna with EBG structures for 5G applications," in *Proc. 2015 Int. Conf. Inf. Commun. Technol. Res. ICTRC 2015*, pp. 5–8, 2015.

[11] C. Rahul, S. Debdeep, G. Debarati, S. Chinmoy, J. Y. Siddiqui, and Y. M. M. Antar, "Four element MIMO antenna system based on SRR loaded printed monopoles for 28/38 GHz 5G applications," in *Proc. 2020 Int. Symp. Antennas Propagation, APSYM 2020*, pp. 36–39, 2020.

[12] S. Tariq, S. I. Naqvi, N. Hussain, and Y. Amin, "A Metasurface-based MIMO antenna for 5G millimeter-wave applications," *IEEE Access*, vol. 9, pp. 51805–51817, 2021.

[13] H. Wang, L. Liu, Z. Zhang, Y. Li, and Z. Feng, "A wideband compact WLAN/WiMAX MIMO antenna based on dipole with V-shaped ground branch," *IEEE Trans. Antennas Propag.*, vol. 63, no. 5, pp. 2290–2295, 2015.

[14] R. Anitha, P. V. Vinesh, K. C. Prakash, P. Mohanan, and K. Vasudevan, "A compact quad element slotted ground wideband antenna for MIMO applications," *IEEE Trans. Antennas Propag.*, vol. 64, no. 10, pp. 4550–4553, 2016.

[15] M. Usman, E. Kobal, J. Nasir, Y. Zhu, C. Yu, and A. Zhu, "Compact SIW fed dual-port single element annular Slot MIMO antenna for 5G mmWave applications," *IEEE Access*, vol. 9, pp. 91995–92002, 2021.

[16] W. Ali, S. Das, H. Medkour, and S. Lakrit, "Planar dual-band 27/39 GHz millimeter-wave MIMO antenna for 5G applications," *Microsyst. Technol.*, vol. 27, no. 1, pp. 283–292, 2021.

[17] R. Sharma, R. Khanna, and Geetanjali, "Compact Sub-6 GHz and mmWave 5G wideband 2 × 1 MIMO antenna with high isolation using parasitically placed double negative (DNG) isolator," *Wirel. Pers. Commun.*, vol. 122, no. 3, pp. 2839–2857, 2022.

[18] M. A. Salamin, N. Hussain, and T. T. Le, "A 2 × 1 array-based wideband mm-wave antenna integrated with a 2-element multiple-input-multiple-output antenna for 5G mobile terminals," *Int. J. RF Microw. Comput. Eng.*, vol. 31, no. 8, pp. 1–13, 2021.

[19] B. T. P. Madhav, Y. Usha Devi, and T. Anilkumar, "Defected ground structured compact MIMO antenna with low mutual coupling for automotive communications," *Microw. Opt. Technol. Lett.*, vol. 61, no. 3, pp. 794–800, 2019.

[20] A. Patel *et al.*, "UWB CPW fed 4-port connected ground MIMO antenna for sub-millimeter-wave 5G applications," *Alexandria Eng. J.*, vol. 61, no. 9, pp. 6645–6658, 2022.

[21] D. El Khamlichi, N. A. Touhami, T. Elhamadi, and M. Ali Ennasar, "High-gain and broadband SIW cavity-backed slots antenna for X-band applications," *Int. J. Microw. Wirel. Technol.*, vol. 13, no. 10, pp. 1078–1085, 2021.

[22] F. Juma'a and F. Alnahwi, "Design and Simulation of a Compact Filtenna for 5G Mid-Band Applications," *Iraqi J. Electron. Electron. Eng.*, vol. 6, no. 2, pp. 52–57, 2021.

[23] M. Shahpari and D. V. Thiel, "Fundamental limitations for antenna radiation efficiency," *IEEE Trans. Antennas Propag.*, vol. 66, no. 8, pp. 3894–3901, 2018.

[24] F. Urimubenshi, D. B. O. Konditi, J. de Dieu Iyakaremye, P. M. Mpele, and A. Munyaneza, "A novel approach for low mutual coupling and ultra-compact two port MIMO antenna development for UWB wireless application," *Heliyon*, vol. 8, no. 3, p. e09057, 2022.

[25] Y. L. Ban, C. Li, C. Y. D. Sim, G. Wu, and K. L. Wong, "4G/5G multiple antennas for future multi-mode smartphone applications," *IEEE Access*, vol. 4, no. c, pp. 2981–2988, 2016.

[26] A. A. Megahed, M. Abdelazim, E. H. Abdelhay, and H. Y. M. Soliman, "Sub-6 GHz highly isolated wideband MIMO antenna arrays," *IEEE Access*, vol. 10, pp. 19875–19889, 2022.

[27] W. A. Neamah, H. M. Al Sabbagh, and H. Al-Rizzo, "New design of a compact 1×2 Super UWB-MIMO antenna for polarization diversity," *Iraqi J. Electron. Electron. Eng.*, vol. 19, no. 1, pp. 111–118, 2023.
[28] N. Hussain, G. S. Member, and M. Jeong, "Metasurface-based single-layer wideband circularly polarized MIMO antenna for 5G millimeter-wave systems," *IEEE Access*, vol. 8, 2020.
[29] A. W. M. Saadh, K. Ashwath, P. Ramaswamy, T. Ali, and J. Anguera, "A uniquely shaped MIMO antenna on FR4 material to enhance isolation and bandwidth for wireless applications," *AEU - Int. J. Electron. Commun.*, vol. 123, p. 153316, 2020.
[30] M. Khalid *et al.*, "4-port MIMO antenna with defected ground structure for 5G millimeter-wave applications," *Electron.*, vol. 9, no. 1, 2020.
[31] M. N. Hasan, S. Bashir, and S. Chu, "Dual-band omnidirectional millimeter wave antenna for 5G communications," *J. Electromagn. Waves Appl.*, vol. 33, no. 12, pp. 1581–1590, 2019.
[32] A. R. Sabek, W. A. E. Ali, and A. A. Ibrahim, "Minimally coupled two-element MIMO antenna dual-band (28/38 GHz) for 5G wireless communications," *J. Infrared, Millimeter, Terahertz Waves*, no. 0123456789, 2022.
[33] D. E. Hadri, A. Zugari, and A. Zakriti, "Extra wide band MIMO antenna with high isolation and low correlation at 38 GHz mm-wave frequency band for 5G applications," *E3S Web Conf.*, vol. 351, p. 01076, 2022.
[34] M. M. Fakharian, M. Alibakhshikenari, C. H. See, and R. Abd-Alhameed, "A high gain multi-band offset MIMO antenna based on a planar log-periodic array for Ku/K-band applications," *Sci. Rep.*, vol. 12, no. 1, pp. 1–13, 2022.
[35] B. A. Esmail and S. Koziel, "High isolation metamaterial-based dual-band MIMO antenna for 5G millimeter-wave applications," *AEU - Int. J. Electron. Commun.*, vol. 158, p. 154470, 2023.
[36] A. Ahmad, D. Y. Choi, and S. Ullah, "A compact two elements MIMO antenna for 5G communication," *Sci. Rep.*, vol. 12, no. 1, pp. 1–8, 2022.